Earth Systems and Environment (2024) 8:45–61
https://doi.org/10.1007/s41748-023-00363-z

ORIGINAL ARTICLE

Impact of the El Niño on Fire Dynamics on the African Continent

José Francisco de Oliveira-Júnior[1] · David Mendes[2] · Szilard Szabo[3] · Sudhir Kumar Singh[4] · Punyawi Jamjareegulgarn[5] · Kelvy Rosalvo Alencar Cardoso[1] · Laszlo Bertalan[3] · Marcos Vinicius da Silva[6] · Alexandre Maniçoba da Rosa Ferraz Jardim[7] · Jhon Lennon Bezerra da Silva[7] · Gustavo Bastos Lyra[6] · Marcel Carvalho Abreu[6] · Washington Luiz Félix Correia Filho[8] · Amaury de Sousa[9] · Dimas de Barros Santiago[10] · Iwldson Guilherme da Silva Santos[10] · Vafaeva Khristina Maksudovna[11]

Received: 13 August 2023 / Revised: 12 November 2023 / Accepted: 24 November 2023 / Published online: 3 January 2024

Abstract

Several studies investigated the occurrence of fires in Africa with numerical modeling or applied statistics; however, only a few studies focused on the influence of El Niño on the fire risk using a coupled model. The study aimed to assess the influence of El Niño on wildfire dynamics in Africa using the SPEEDY-HYCOM model. El Niño events in the Eastern Tropical Pacific were classified via sea surface temperature (SST) anomaly based on a predefined climatology between 1961 and 2020 for the entire time series of SST, obtaining linear anomalies. The time series of the SST anomalies was created for the region between 5° N and 5° S and 110° W and 170° W. The events were defined in three consecutive 3-month periods as weak, moderate, and strong El Niño conditions. The Meteorological Fire Danger Index (MFDI) was applied to detect fire hazards. The MFDI simulated by the SPEEDY-HYCOM model for three El Niño categories across different lagged months revealed relevant distinctions among the categories. In the case of 'Weak', the maximum variability of fire risk observed at time lags (0, -3, -6, and -9 months) was primarily in Congo, Gabon, and Madagascar. The 'Moderate' pattern had similar characteristics to 'Weak' except for the lag-6 months and its occurrence in the equatorial zone of Africa. 'Strong' showed a remarkable impact in East Africa, resulting in high fire risk, regardless of time lags. Precipitation and evaporation simulations (SPEEDY-HYCOM) indicated that El Niño categories in Africa need particular attention in the central, southern, and southeastern regions emphasizing the significance of lag-0 and lag-6 (evaporation) as well as lag-0, lag-6, and lag-9 (precipitation). The SPEEDY-HYCOM coupled model in conjunction with the MFDI was efficient in assessing climate variabilities in Africa during El Niño events. This model allows the analysis and prediction of wildfire risks based on El Niño events, providing crucial information for wildfire management and prevention. Its simulations uncover significant variations in risks among different El Niño categories and lagged months, contributing to the understanding and mitigation of this environmental challenge.

Keywords Fire risk · Coupled modeling · El Niño categories · SPEEDY-HYCOM model

1 Introduction

The El Niño-Southern Oscillation (ENSO) climate variability mode is a phenomenon of ocean–atmosphere interaction that occurs in the Tropical Pacific Ocean and is considered the primary driver of climate variability in various regions of the Earth (Trenberth 1997; Philander 1998; Adamson 2022). ENSO has two distinct phases: a warm phase known as El Niño and a cold phase known as La Niña (Berlato et al. 2005; Abreu et al. 2023).

Between 2015 and 2016, El Niño was one of the strongest in history (Varotsos et al. 2016; Burton et al. 2020) and was called a Mega El Niño due to the increase in extreme droughts in various regions of the world (Jimenez et al. 2018; Xie et al. 2022). Drought is a primary factor of wildfire and its increasing frequency projects a higher risk of fires, too. Understanding the dynamics of fires in arid areas, e.g., in Africa, is crucial for comprehending ecosystem properties and their impact on the global carbon (C) cycle (Wei et al. 2020). Furthermore, fires are significant in African ecosystems (Trollope and Trollope 1997; Bowman et al. 2009; Ribeiro et al. 2019), with the continent responsible

Extended author information available on the last page of the article

for 70% of the global burned area (Russell-Smith et al. 2021) and 50% of C emissions related to fire (Giglio et al. 2013; Jiang et al. 2020). Arid lands cover 43% of the African continent and play a critical role in the C cycle and the livelihoods impacted by wildfires (Wei et al. 2021; Russell-Smith et al. 2021). Africa is known as the "Continent of Fire" and can be characterized by extensive biomass burning (Trollope and Trollope 1997; Strydom and Savage 2016). Fires represent crucial factors affecting ecosystem processes (Ribeiro et al. 2019), especially in grassland areas (Cao et al. 2015), followed by impacts on biogeochemical cycles, vegetation dynamics, and interference with Africa's climate conditions (Sedano et al. 2020; Russell-Smith et al. 2021).

Many factors contribute to fires in the African continent, such as population density, season (i.e., only 5% of wildfires occur in the rainy season), vegetation type (e.g., grasslands, shrublands, savannas, and forests), vegetation state (phenology; dry or wet; alive or dead), and landscape connectivity (hindering or facilitating spread), but the role of rainfall pattern stands out and determines fire variability (Archibald et al. 2009, 2011; Strydom and Savage 2016; Russell-Smith et al. 2021; Loudermilk et al. 2022).

According to satellite data and statistical models, Andela and Van der Werf (2014) found that changes in the rainfall patterns during the transition from El Niño to La Niña accounted for 51% of the increase in fires in Southern Africa. They demonstrated that rapidly changing demographic and socioeconomic situations have led to a significant increase in the area burned due to the conversion of savannas into agricultural lands. Burton et al. (2020) utilized the coupled fire-vegetation model JULES-INFERNO to investigate the impact of the 2015/16 Mega El Niño on fires in South America, Africa, and Asia, but the model did not accurately represent the increase in burned areas during El Niño conditions in Africa.

Numerous studies have already been conducted on fires in Africa from numerical modeling and the impact of rainfall (De Sales et al. 2019; Strydom and Savage 2016; Burton et al. 2020), followed by applied statistics (Andela and van der Werf 2014; Ribeiro et al. 2014, 2020) to the use of satellite products (Chen et al. 2017; Saha et al. 2019; Jiang et al. 2020; Sedano et al. 2020; Wan and Roy 2022) and risk analysis (Ansari et al. 2023a, b). However, only a few studies have exclusively addressed the influence of El Niño and its categories on fire risk based on a coupled ocean–atmosphere model along with a fire risk index, which represents a novel methodology applied to the African continent.

The SPEEDY-HYCOM climate model offers several advantages over other climate models, such as its high flexibility and applicability to various environmental problems (Oliveira-Júnior et al. 2021; Gobbo et al. 2022). In many aspects, SPEEDY-HYCOM can match or even outperform state-of-the-art models in simulating climate means and variability, especially large-scale features (Kucharski et al. 2005; Kotsuki et al. 2022). The model is effective in investigating the sensitivity of simulated climate to changes in parameters within physical parameterization, which is crucial to understanding how different factors affect the climate (Held and Suarez 1978; Molteni 2003). Recently, the model has been used in studies on wildfire meteorology (Xu et al. 2016; Oliveira-Júnior et al. 2021).

Therefore, our research aimed to (i) investigate the potentiality of coupled SPEEDY-HYCOM model for wildfires and (ii) evaluate the influence of El Niño events on the dynamics of wildfires in Africa via the coupled SPEEDY-HYCOM model. The results shed light on vegetation burning in Africa and its complex interrelationships between fire, climate, and human activity. The findings from this research process provide valuable insights and point to several important considerations for sustainable fire management and the reduction of pollutant emissions.

2 Material and Methods

2.1 Study Area

Africa is a continent of about 30 million km^2, accounting for 20.3% of the planet. It is the second most populous continent on Earth, represented by 54 countries (Fig. 1)—(Spinoni et al. 2021). The African continent is bounded by the Mediterranean Sea to the north (N), the Isthmus of Suez and the Red Sea to the northeast (NE), the Indian Ocean to the southeast (SW), and the Atlantic Ocean to the west (W). In addition to the main continent, Africa includes Madagascar and several archipelagos (Thomson 2022). Africa is the hottest continent on Earth, with approximately 60% of its land area consisting of arid lands and deserts (Griffiths 2013). According to the Köppen–Geiger climate classification map (Fig. 1), the tropical zone (rainforest and savanna) prevails between the N11° and S11° latitudes, but larger areas belong to the arid zones (deserts, semi-arid areas, and steppes) with increased risk of wildfires.

2.2 SPEEDY-HYCOM Coupled Model

The Simplified Parametrization, primitivE-Equation DYnamics (SPEEDY) model is a spectral and hydrostatic atmospheric model, with eight layers (30, 100, 200, 300, 500, 700, 850, and 925 hPa—hectopascal) in sigma coordinates, with a horizontal truncation of T30, this corresponds to a horizontal resolution of approximately 3.95 degrees in both latitude and longitude (Gobo et al. 2022). For the implementation of the SPEEDY model, the following variables were added: long-wave radiation (LWR) and short-wave radiation (SWR), large-scale

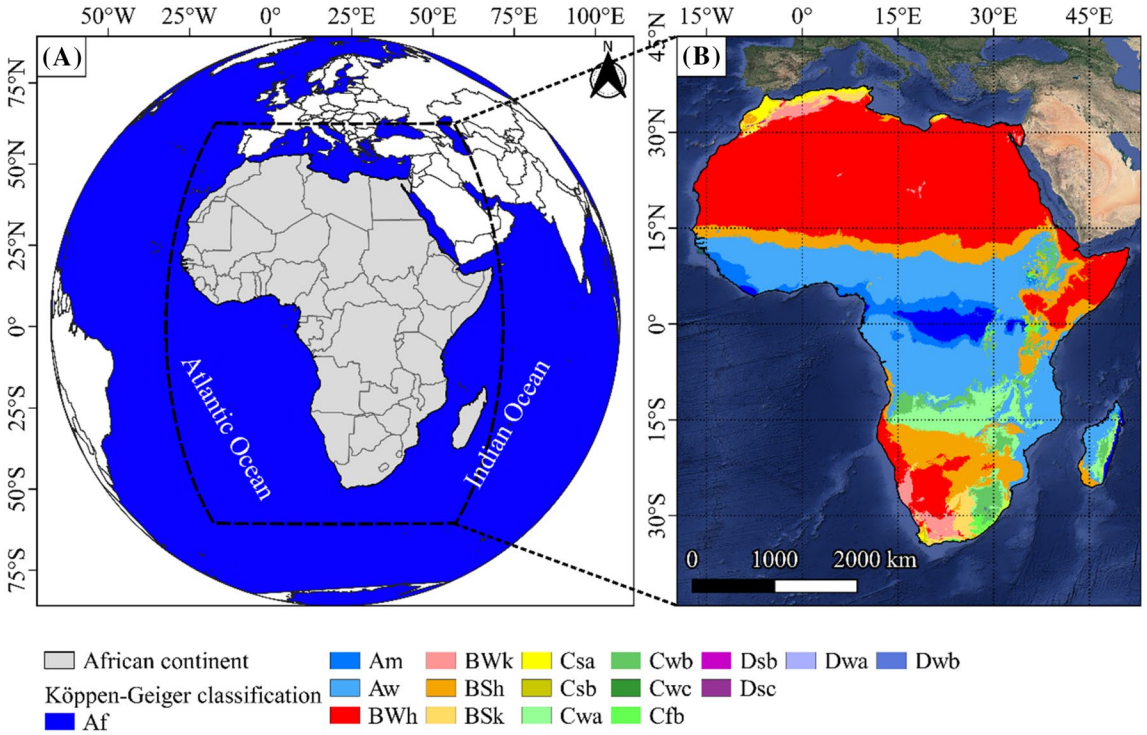

Fig. 1 African continent, with the Köppen–Geiger climate classification. (Source: set of climate maps, spatial resolution of 1 km, topographically corrected 1980–2016, Beck et al. 2018)

condensation, convection heat flux, latent heat flux, moisture, and momentum, as well as vertical diffusion processes (Held and Suarez 1978; Molteni 2003). SPEEDY offers computational advantages by having its processing twice as fast as other climate models of the same horizontal resolution. In this way, it allows for carrying out experiments on distinct scales, such as interannual, decennial, and even secular (Kotsuki et al. 2022). In addition to the advantages previously presented, the SPEEDY model reproduces climate system characteristics regardless of the region (tropical, middle, and high latitudes) (Kucharski et al. 2005).

The Hybrid Coordinate Ocean Model (HYCOM) is a model version of ocean circulation in hybrid coordinates from MICOM (Miami Isopycnic Coordinate Ocean Model) and was developed to simulate the global ocean circulation, as well as mesoscale and coastal processes, in addition to solving equations of momentum, mass, and energy balance in hybrid vertical coordinates (Bleck 2002). HYCOM uses the coordinates hybrid, as the ocean has columns of water that are not stratified, or unstable convection from International Comprehensive Ocean–Atmosphere Data Set. These coordinates allow a better transition from the mixed layer (ML) to greater ocean depth (Bleck 2002).

2.3 SPEEDY-HYCOM Model Simulations

The first-year simulation began in January 1960 due to the initial spin-up to stabilize the model and not bring noise to the simulation process. Restoring the boundary conditions is useful when seeking balance for oceanic models, in which the temperature and surface salinity must follow the data from model input. Similarly, they are also used in models of atmospheric conditions when sea surface temperature (SST, °C) is prescribed. For such SST conditions, we used the Extended Reconstructed Sea Surface Temperature (ERSST), which is a global monthly analysis of SST data derived from the International Comprehensive dataset Ocean–Atmosphere Dataset (ICOADS) (Huang et al. 2020).

In the context of heat fluxes, a plausible argument can be made that these fluxes are proportional to the deviations. This concept aligns with the formulation of heat flow described in Fick's 1st law. In physical terms, for example, an SST warm anomaly leads to increased heat flow from ocean to the atmosphere. It, therefore, leads to ocean cooling, which tends to restore the previous equilibrium condition. To initialize the SPEEDY-HYCOM model, we utilized initial conditions such as sea surface temperature climatology (SST, °C), temperature at 2 m above ground (°C), precipitation (mm.day^{-1}), evaporation (mm.day^{-1}), and albedo

(%). All of these data are derived from the NCEP/NCAR reanalysis (Kalnay et al. 1996) and covers the period from 1979 to 2015.

2.4 El Niño Classification

El Niño events in the Eastern Tropical Pacific were classified via SST anomaly based on a predefined climatology between 1961 and 2020 for the entire time series of SST, obtaining linear anomalies. The series time of the SST anomalies was created for the region between 5° N and 5° S and 110° W and 170° W. Events were defined in three consecutive periods of three months, superimposed on values above 0.55 °C, being called El Niño events. The events were defined in three consecutive three-month periods, overlaid on values above 0.55 °C, and were referred to as El Niño events. The event thresholds were classified as follows: (i) weak, with an SST anomaly between 0.55 °C and 0.95 °C; (ii) moderate, with an SST anomaly between 0.96 °C and 1.45 °C; and (iii) strong, with an SST anomaly exceeding 1.45 °C (Table 1). The classification was based on simulations of the coupled ocean–atmosphere model SPEEDY-HYCOM.

2.5 Meteorological Fire Danger Index (MFDI)

The MFDI was used in the study to assess fire hazards in Africa. The MDFI represents how predisposed vegetation should be burned, as the longer the time without rain (summer weather and/or prolonged drought), the greater the risk of vegetation burning (Camia et al. 1999; Vitolo et al. 2020). The calculation of the MFDI consists of information on vegetation cover and values daily maximum air temperature (Tmax, ºC), minimum relative humidity (RH min, %), and accumulated rainfall (P, mm) of the site.

The Drought Day Index (DD) is calculated daily based on the product of 11 precipitation factors taking into account accumulated precipitation over 11 previous periods (days) (Eq. 1 and Table 2)

$$\mathrm{DD} = \prod_{i=1}^{11} \exp\left(-\beta_i, P_i\right), \tag{1}$$

where β_i is the decay factor, and P_i represents the accumulated precipitation in millimeters (mm).

The Base Danger (BD) was estimated for each day by combining DD for that day with a sinusoidal curve representing the effects of phenology for different types of vegetation, as per Eq. (2)

$$\mathrm{BD} = 0.45(1 + \sin(\min(A \times \mathrm{DD}, 180°) - 90°)). \tag{2}$$

In this context, the argument of the sinusoidal function is measured in degrees, and the coefficient values for 'A' are 2.4 for closed savanna and closed forest, and 3.0 for savanna and open forest. The rationale for using BD is that, for the same DD value, the fire danger is higher.

The effects of relative humidity and air temperature were also taken into account for each day through the so-called Humidity Factor (HF) and the Temperature Factor (TF), defined in Eqs. (3) and (4)

$$\mathrm{HF} = -0.006 \times \mathrm{RH} + 1.3 \tag{3}$$

$$\mathrm{TF} = 0.02 \times T + 0.4, \tag{4}$$

where HF is the Humidity Factor, RH is the Relative Humidity, TF is the Temperature Factor, and T is Surface Air Temperature. Fire danger increases (decreases) when relative humidity is lower (higher) than 40%. Temperature has a linear relation with the risk increasing when the temperature exceeds 30 °C.

For each day, the value of MFDI is obtained by multiplying the Base Danger by the Moisture and Temperature Factors, as per Eq. (5) and Table 3

$$\mathrm{MFDI} = \mathrm{BD} \times \mathrm{TF} \times \mathrm{HF}. \tag{5}$$

The methodology used in the study is summarized in Fig. 2.

3 Results

3.1 Fire Risk Modeling

By simulating the MFDI in lagged months, according to the Weak ENSO category (Fig. 3), we identified the variability of the maximum risk (high and very high) in the time lags. Based on lag-0, which represents the maximum peak period in ENSO (Fig. 3a), the maximum risk of MFDI identified was concentrated in the equatorial belt and in Southern Africa with a higher risk of fire in the following countries: Congo, Gabon, and Madagascar. Up to 3 months before the peak of an ENSO Weak (Fig. 3b), there was a decrease in the moderate risk area and an expansion of the very high-risk area. The very high risk expanded to West (W) African countries, thus, delimiting a wide and homogeneous range of forest fires. Furthermore, the region around the South of Southern Africa practically became less sensitive in terms of MFDI. Six months before the peak of Weak ENSO (Fig. 3c), there was an expansion of maximum risk to the North (N) of the continent and again no risk to the S of Southern Africa. For 9 months before the peak of ENSO (Fig. 3d), a condition of stabilization occurred in the region where there was a maximum risk, concentrated in the equatorial belt of the continent and expansion of moderate areas and weak for S southern Africa.

Table 1 Classification of El Niño extremes via SST anomaly simulated by the SPEEDY-HYCOM model. El Niño types are Weak (W), Moderate (M), and Strong (S)

ENSO		Months											
Type	Season	JJA	JAS	ASO	SON	OND	NDJ	DJF	JFM	FMA	MAM	AMJ	MJJ
	1959-1960	-0.2	-0.3	-0.1	0.0	0.0	0.0	-0.1	-0.1	-0.1	0.0	0.0	0.0
	1960-1961	0.1	0.2	0.3	0.2	0.1	0.1	0.0	0.0	0.0	0.1	0.2	0.3
	1961-1962	0.1	-0.1	-0.3	-0.3	-0.2	-0.2	-0.2	-0.2	-0.2	-0.3	-0.3	-0.2
	1962-1963	0.0	-0.1	-0.1	-0.2	-0.3	-0.4	-0.4	-0.2	0.2	0.3	0.3	**0.5**
M	1963-1964	**0.9**	**1.1**	**1.2**	**1.3**	**1.4**	**1.3**	**1.1**	**0.6**	0.1	-0.3	-0.6	-0.6
	1964-1965	-0.6	-0.7	-0.8	-0.8	-0.8	-0.8	-0.6	-0.3	-0.1	0.2	**0.5**	**0.8**
S	1965-1966	**1.2**	**1.5**	**1.9**	**2.0**	**2.0**	**1.7**	**1.4**	**1.2**	**1.0**	**0.7**	0.4	0.2
	1966-1967	0.2	0.1	-0.1	-0.1	-0.2	-0.3	-0.4	-0.5	-0.5	-0.4	-0.2	0.0
	1967-1968	0.0	-0.2	-0.3	-0.4	-0.3	-0.4	-0.6	-0.7	-0.6	-0.4	0.0	0.3
M	1968-1969	0.6	0.5	0.4	**0.5**	**0.7**	**1.0**	**1.1**	**1.1**	**0.9**	**0.8**	**0.6**	**0.4**
W	1969-1970	**0.4**	**0.5**	**0.8**	**0.9**	**0.8**	**0.6**	**0.5**	0.3	0.3	0.2	0.0	-0.3
	1970-1971	-0.6	-0.8	-0.8	-0.7	-0.9	-1.1	-1.4	-1.4	-1.1	-0.8	-0.7	-0.7
	1971-1972	-0.8	-0.8	-0.8	-0.9	-1.0	-0.9	-0.7	-0.4	0.1	0.4	**0.7**	**0.9**
S	1972-1973	**1.1**	**1.4**	**1.6**	**1.8**	**2.1**	**2.1**	**1.8**	**1.2**	**0.5**	-0.1	-0.5	-0.9
	1973-1974	-1.1	-1.3	-1.5	-1.7	-1.9	-2.0	-1.8	-1.6	-1.2	-1.0	-0.9	-0.8
	1974-1975	-0.5	-0.4	-0.4	-0.6	-0.8	-0.6	-0.5	-0.6	-0.7	-0.7	-0.8	-1.0
	1975-1976	-1.1	-1.2	-1.4	-1.4	-1.6	-1.7	-1.6	-1.2	-0.7	-0.5	-0.3	0.0
W	1976-1977	0.2	0.4	**0.6**	**0.8**	**0.9**	**0.8**	**0.7**	**0.6**	0.3	0.2	0.2	0.3
W	1977-1978	0.4	0.4	**0.6**	**0.7**	**0.8**	**0.8**	**0.7**	0.4	0.1	-0.2	-0.3	-0.3
	1978-1979	-0.4	-0.4	-0.4	-0.3	-0.1	0.0	0.0	0.1	0.2	0.3	0.2	0.0
W	1979-1980	0.0	0.2	0.3	**0.5**	**0.5**	**0.6**	**0.6**	**0.5**	0.3	0.4	0.5	0.5
	1980-1981	0.3	0.0	-0.1	0.0	0.1	0.0	-0.3	-0.5	-0.5	-0.4	-0.3	-0.3
	1981-1982	-0.3	-0.2	-0.2	-0.1	-0.2	-0.1	0.0	0.1	0.2	**0.5**	**0.7**	**0.7**
S	1982-1983	**0.8**	**1.1**	**1.6**	**2.0**	**2.2**	**2.2**	**2.2**	**1.9**	**1.5**	**1.3**	**1.1**	**0.7**
	1983-1984	0.3	-0.1	-0.5	-0.8	-1.0	-0.9	-0.6	-0.4	-0.3	-0.4	-0.5	-0.4
	1984-1985	-0.3	-0.2	-0.2	-0.6	-0.9	-1.1	-1.0	-0.8	-0.8	-0.8	-0.8	-0.6
	1985-1986	-0.5	-0.5	-0.4	-0.3	-0.3	-0.4	-0.5	-0.5	-0.3	-0.2	-0.1	0.0
M	1986-1987	0.2	0.4	**0.7**	**0.9**	**1.1**	**1.2**	**1.2**	**1.2**	**1.1**	**0.9**	**1.0**	**1.2**
S	1987-1988	**1.5**	**1.7**	**1.6**	**1.5**	**1.3**	**1.1**	**0.8**	**0.5**	0.1	-0.3	-0.9	-1.3
	1988-1989	-1.3	-1.1	-1.2	-1.5	-1.8	-1.8	-1.7	-1.4	-1.1	-0.8	-0.6	-0.4
	1989-1990	-0.3	-0.3	-0.2	-0.2	-0.2	-0.1	0.1	0.2	0.3	0.3	0.3	0.3
	1990-1991	0.3	0.4	0.4	0.3	0.4	0.4	0.4	0.3	0.2	0.3	**0.5**	**0.6**
S	1991-1992	**0.7**	**0.6**	**0.6**	**0.8**	**1.2**	**1.5**	**1.7**	**1.6**	**1.5**	**1.3**	**1.1**	**0.7**
	1992-1993	0.4	0.1	-0.1	-0.2	-0.3	-0.1	0.1	0.3	0.5	0.7	0.7	0.6
	1993-1994	0.3	0.3	0.2	0.1	0.0	0.1	0.1	0.1	0.2	0.3	0.4	0.4
M	1994-1995	0.4	0.4	**0.6**	**0.7**	**1.0**	**1.1**	**1.0**	**0.7**	**0.5**	0.3	0.1	0.0
	1995-1996	-0.2	-0.5	-0.8	-1.0	-1.0	-1.0	-0.9	-0.8	-0.6	-0.4	-0.3	-0.3
	1996-1997	-0.3	-0.3	-0.4	-0.4	-0.4	-0.5	-0.5	-0.4	-0.1	0.3	**0.8**	**1.2**
S	1997-1998	**1.6**	**1.9**	**2.1**	**2.3**	**2.4**	**2.4**	**2.2**	**1.9**	**1.4**	**1.0**	**0.5**	-0.1
	1998-1999	-0.8	-1.1	-1.3	-1.4	-1.5	-1.6	-1.5	-1.3	-1.1	-1.0	-1.0	-1.0
	1999-2000	-1.1	-1.1	-1.2	-1.3	-1.5	-1.7	-1.7	-1.4	-1.1	-0.8	-0.7	-0.6
	2000-2001	-0.6	-0.5	-0.5	-0.6	-0.7	-0.7	-0.7	-0.5	-0.4	-0.3	-0.3	-0.1
	2001-2002	-0.1	-0.1	-0.2	-0.3	-0.3	-0.3	-0.1	0.0	0.1	0.2	0.4	**0.7**
M	2002-2003	**0.8**	**0.9**	**1.0**	**1.2**	**1.3**	**1.1**	**0.9**	**0.6**	0.4	0.0	-0.3	-0.2
	2003-2004	0.1	0.2	0.3	0.3	0.4	0.4	0.4	0.3	0.2	0.2	0.2	0.3
W	2004-2005	**0.5**	**0.6**	**0.7**	**0.7**	**0.7**	**0.7**	**0.6**	**0.6**	**0.4**	0.4	0.3	0.1
	2005-2006	-0.1	-0.1	-0.1	-0.3	-0.6	-0.8	-0.8	-0.7	-0.5	-0.3	0.0	0.0
W	2006-2007	0.1	0.3	**0.5**	**0.7**	**0.9**	**0.9**	**0.7**	0.3	0.0	-0.2	-0.3	-0.4
	2007-2008	-0.5	-0.8	-1.1	-1.4	-1.5	-1.6	-1.6	-1.4	-1.2	-0.9	-0.8	-0.5
	2008-2009	-0.4	-0.3	-0.3	-0.4	-0.6	-0.7	-0.8	-0.7	-0.5	-0.2	0.1	0.4
M	2009-2010	**0.5**	**0.5**	**0.7**	**1.0**	**1.3**	**1.6**	**1.5**	**1.3**	**0.9**	0.4	-0.1	-0.6
	2010-2011	-1.0	-1.4	-1.6	-1.7	-1.7	-1.6	-1.4	-1.1	-0.8	-0.6	-0.5	-0.4
	2011-2012	-0.5	-0.7	-0.9	-1.1	-1.1	-1.0	-0.8	-0.6	-0.5	-0.4	-0.2	0.1
	2012-2013	0.3	0.3	0.3	0.2	0.0	-0.2	-0.4	-0.3	-0.2	-0.2	-0.3	-0.3
	2013-2014	-0.4	-0.4	-0.3	-0.2	-0.2	-0.3	-0.4	-0.4	-0.2	0.1	0.3	0.2
W	2014-2015	0.1	0.0	0.2	0.4	**0.6**	**0.7**	**0.6**	**0.6**	**0.6**	**0.8**	**1.0**	**1.2**
S	2015-2016	**1.5**	**1.9**	**2.2**	**2.4**	**2.6**	**2.6**	**2.5**	**2.1**	**1.6**	**0.9**	0.4	-0.1
	2016-2017	-0.4	-0.5	-0.6	-0.7	-0.7	-0.6	-0.3	-0.2	0.1	0.2	0.3	0.3
	2017-2018	0.1	-0.1	-0.4	-0.7	-0.8	-1.0	-0.9	-0.9	-0.7	-0.5	-0.2	0.0
W	2018-2019	0.1	0.2	0.5	**0.8**	**0.9**	**0.8**	**0.8**	**0.7**	**0.7**	**0.7**	**0.5**	**0.5**
	2019-2020	0.3	0.1	0.2	0.4	0.5	0.6	0.5	0.5	0.4	0.2	-0.1	-0.3
	2020-2021	-0.4	-0.6	-0.9	-1.2	-1.3	-1.2	-1.1	-0.9	-0.8	-0.7	-0.5	-0.4

The green color indicates: Events were defined in three consecutive periods of 3 months, superimposed on values above 0.55 °C, being called El Niño events

Table 2 Ranges and values of the decay factors for the 11 periods that integrate the Drought Day (DD) index

Period	Range (in days)	Coefficient (β)
1	1	– 0.14
2	2	– 0.07
3	3	– 0.04
4	4	– 0.03
5	5	– 0.02
6	6	– 0.01
7	7	– 0.008
8	8	– 0.004
9	9	– 0.002
10	10	– 0.001
11	11	– 0.0007

Table 3 Classes of meteorological fire danger and respective ranges of the Meteorological Fire Danger (MFDI)

Danger	Range of MFDI
Minimum	< 0.15
Low	0.15–0.40
Medium	0.40–0.70
High	0.70–0.95
Critical	> 0.95

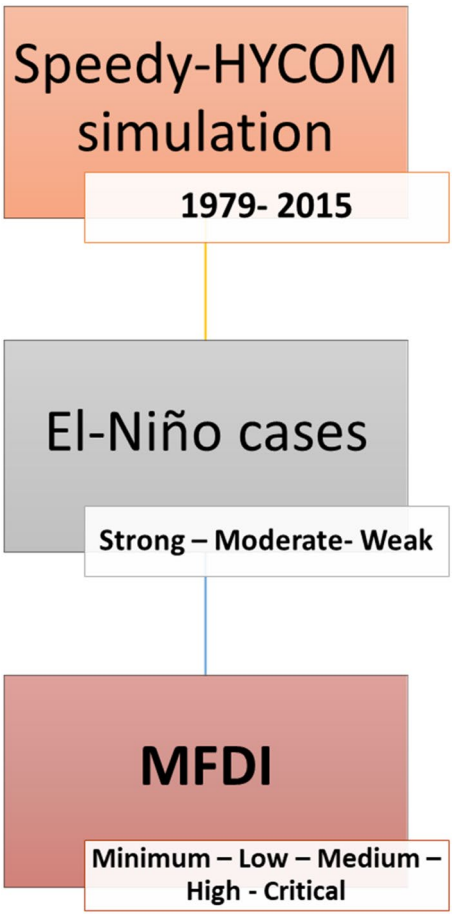

Fig. 2 The flowchart of the methodology applied in the study

Regarding the Moderate ENSO category (Fig. 4), there was a similarity between the previously noted fire risk in the Weak ENSO category (Fig. 3), mainly in relation to spatial variability between time lags where there was a region with a predominance of maximum risk, mainly located in the equatorial belt and migrating to the N, mainly 6 months before the peak of the Moderate ENSO category (Fig. 4c).

Concerning the other two ENSO events, it is important to highlight the important state of the main ENSO category (Fig. 5). The region of East (E) Africa, specifically between Kenya and Somalia had been identified as having the maximum risk according to the MFDI, in all conditions (lag -0, -3, -6, and -9 months; Fig. 5). Extensive undergrowth is prevalent, particularly in the S, Southwest (SW), and E of Africa.

3.2 Influences of Precipitation and Evaporation

Regarding the El Niño Weak lag-0, there was no change in evaporation throughout the continent. In contrast, at lag-3, a positive evaporation anomaly was observed in Central Africa, spanning from the coast to the interior of the continent, with particular emphasis on the countries of Guinea, Ivory Coast, Ghana, and Nigeria. This positive anomaly was followed by negative evaporation rates in Southern Africa, primarily along the border between Zambia, Zimbabwe, Namibia, and Botswana (Fig. 6).

A similar situation was identified in lag-6 in relation to the previously highlighted areas in lag-3, with the intensification of evaporation anomalies. An exception was lag-9 in the El Niño Weak category, with negative anomalies of evaporation in central Africa and positive evaporation anomalies between Namibia and Botswana.

In the context of El Niño events, a comparison between the Moderate and Weak categories revealed relevant differences at lag-0. Specifically, a considerable decrease in evaporation was observed, with an emphasis on negative anomalies occurring across the entire of Central Africa (Fig. 7). The border region shared by Zambia, Zimbabwe, Namibia, and Botswana exhibited the most substantial positive anomalies in evaporation. This contrast becomes particularly evident during lag periods of 3 to 6 months after the El Niño Weak conditions. Concerning the lag-3, there was a reduction in the magnitude

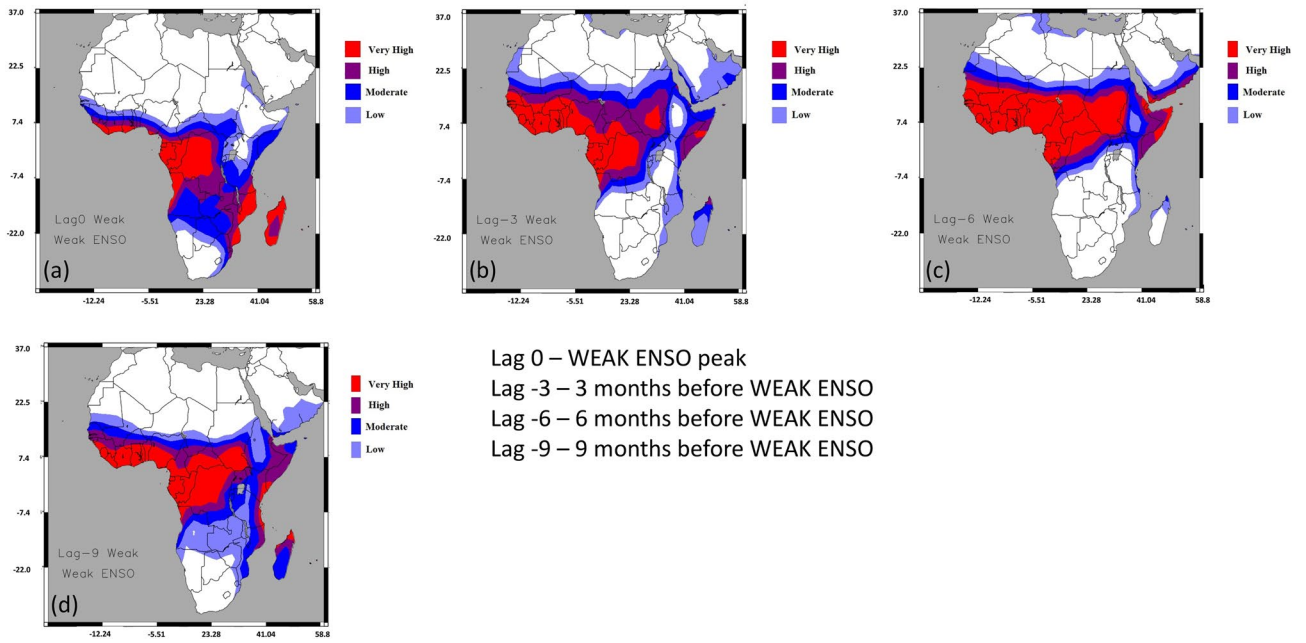

Fig. 3 Simulations with the SPEEDY model for a control period (1961–2021), for weak ENSO regarding the spatial distribution of MFDI and its categories

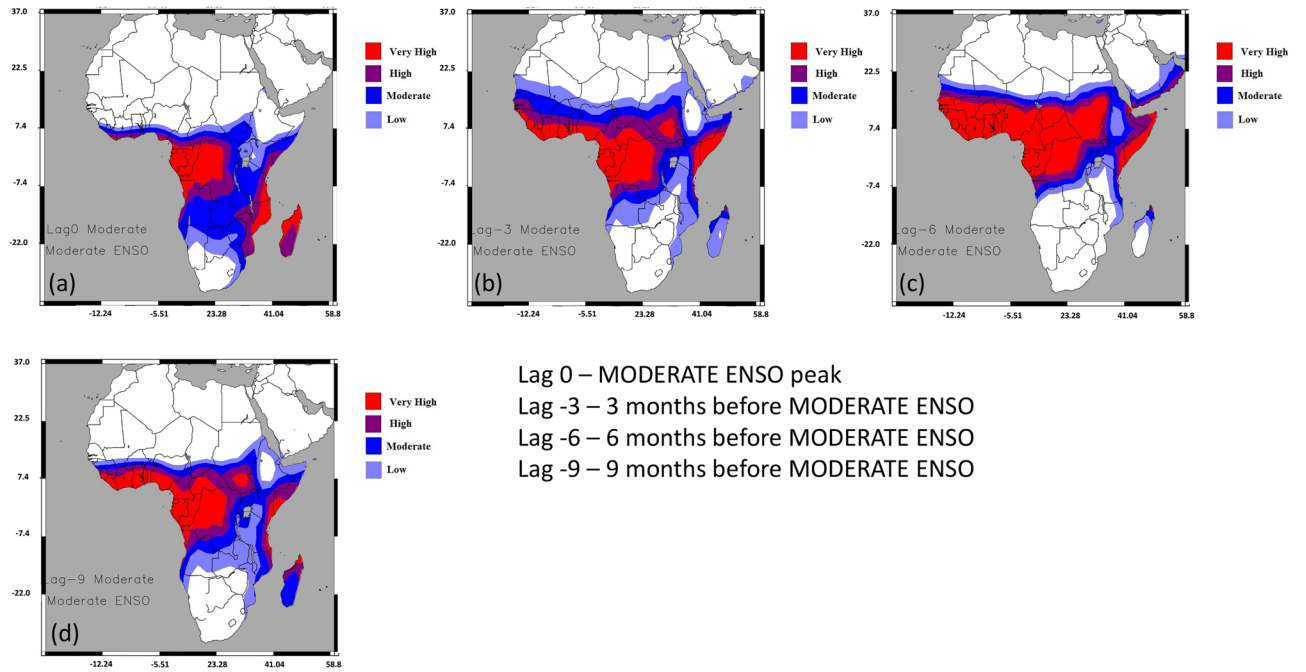

Fig. 4 Simulations with the SPEEDY model for a control period, for Moderate ENSO regarding the spatial distribution of MFDI and its categories

of positive anomalies and a shift to negative effects on evaporation across the continent. This change also corresponds to variations in evaporative patterns compared to the conditions observed during El Niño Moderate at lag-0. Notably, these patterns persist through the lag-6 period. Moreover, the negative anomalies of evaporation of lag-9 can be found in the central areas of Africa

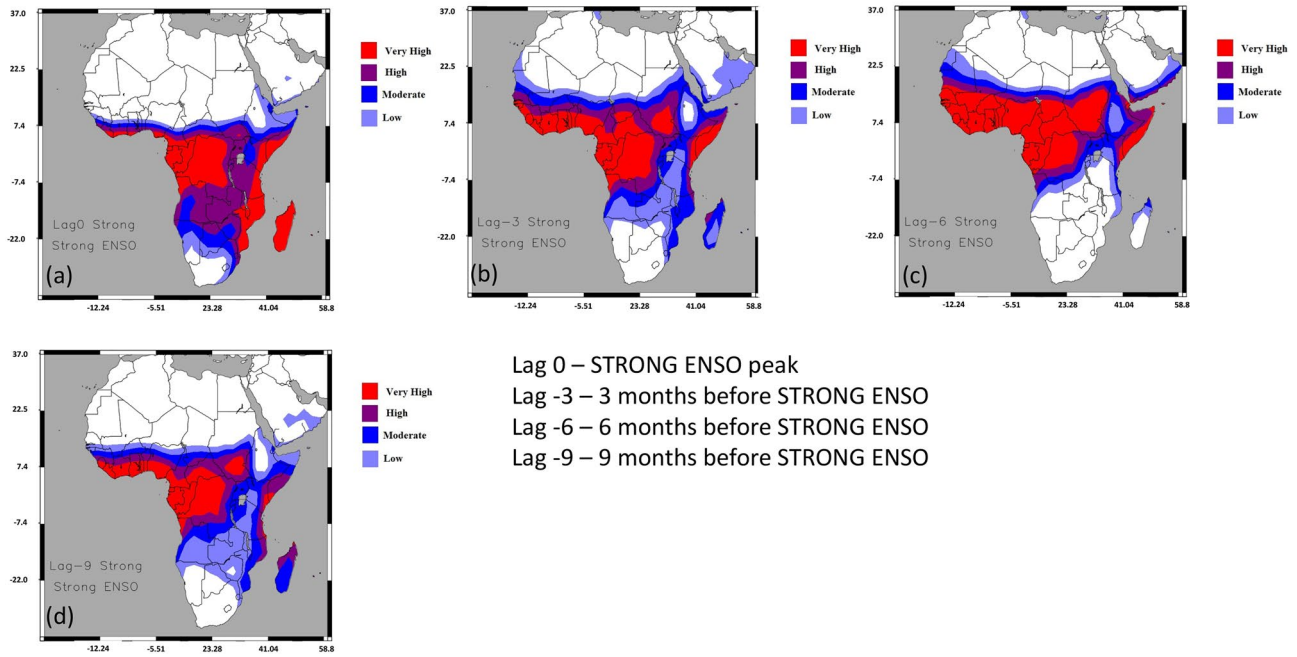

Fig. 5 Simulations with the SPEEDY model for a control period, for Strong ENSO regarding the spatial distribution of MFDI and its categories

without the occurrence of positive anomalies of evaporation as in the Weak El Niño category.

The El Niño Strong category lag-0 indicated a higher occurrence of negative evaporation anomalies compared to the other categories, again highlighting Central Africa (Fig. 8). In lag-3 of El Niño Strong, there was a significant decrease in evaporation, unlike the other categories of El Niño. In the El Niño Strong lag-6 positive anomalies of evaporation in Central Africa and negative evaporation anomalies between Angola and the Congo. In lag-9, negative evaporation anomalies were observed off the coast of Africa, particularly affecting regions such as Gambia, Guinea-Bissau, and Mali. Conversely, positive anomalies occurred in Tanzania.

There was no change concerning lag-0 and lag-3 of the El Niño Weak in precipitation across the continent except Sudan (Fig. 9). Regarding the lag-6 of El Niño peak, the largest positive precipitation anomalies occurred in all of Central Africa. There were minor precipitation records in Central Africa with emphasis on Gambia, Senegal, and mainly Chad and Sudan (Fig. 9).

With the El Niño Moderate lag-0, the lowest precipitation rates across Central Africa as opposed to El Niño lag-0 Weak (Fig. 10). The higher precipitation records can be found obviously in the southern part of Africa, particularly in Madagascar. In lag-3, however, there were lower records of precipitation in some African countries, e.g., Mauritania, Niger, Sudan, Somalia, and the border between Angola and Congo. Regarding lag-6, the highest precipitation rates occurred in all of Central Africa, except in Ethiopia, unlike southern Africa with the lowest rainfall rates, opposite situation of lag-0. Highlight for lag-9 with the lowest rates of precipitation, mainly in Chad and Sudan, similar to El Niño category weak.

There was a significant increase in the smallest records of rainfall in El Niño Strong category for lag-0 as opposed to lag-0 in previous years, followed by a decrease in positive precipitation anomalies in Southern Africa (Fig. 11). It is worth highlighting the similarity between El Niño Strong and El Niño Weak with lags of 3 and 6 months, and the exception was the increase in anomalies of negative rainfall in southern Africa, mainly in Angola and the border between Zambia, Namibia, and Botswana. Furthermore, lag-9 was not similar to the lags of the previous year, it indicated a negative precipitation anomaly in Senegal and Mauritania and a positive precipitation anomaly, only in Tanzania.

4 Discussions

The results obtained from MFDI confirm the previous findings of Andela and van der Werf (2014), which reveal that the trend of burning areas is directly related to ENSO, increasing by 51%. Strydom and Savage (2016) assessed the spatiotemporal distribution of fires in South Africa from 2003 to 2013 using a dataset of MODIS-derived Active Fire Hotspots and found that the eastern and northeastern regions were more susceptible to fires, in contrast to the MFDI,

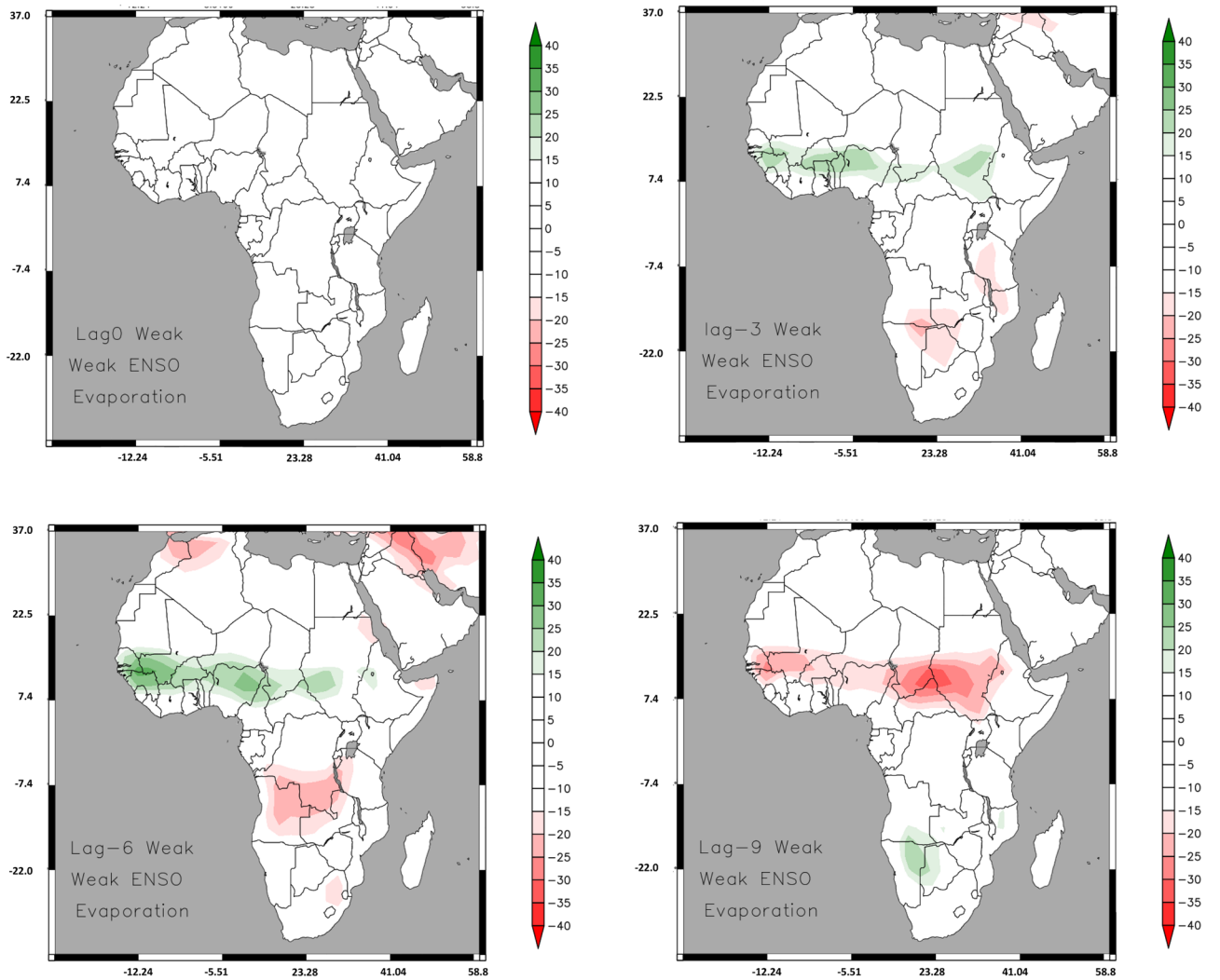

Fig. 6 Evaporation simulations (mm) in the Weak ENSO category

which identified only the northeastern sector. In recent decades, the areas affected by wildfires in South Africa have increased significantly, as indicated by studies by Joshua and Sukumar (2021) and Carter et al. (2021).

It is noteworthy that such countries are densely covered by forest (Ribeiro et al. 2019; Burton et al. 2020; Jiang et al. 2020) and, recently, it was verified via geo-spatialization of the MODIS product MOD14/MYD14 Fire and Thermal Anomalies in the Congo Basin and Forests Mountain ranges on the Northeast (NE) coast of Madagascar (Wan and Roy 2022). The moderate risk category can be found in Southern Africa, mainly in the Kalahari region. Saha et al. (2019) evaluated the impact of fires in the albedo of the terrestrial surface, since the generalized presence of fires in Africa has implications for the regional climate and the hydrological cycle, mainly in the Kalahari region, southern Africa. Previously, Joshi and Sukumar (2021) pointed out that the socio-anthropogenic conditions in Southern Africa exhibit a high positive sensitivity of the burned area to temperature, in contrast to northern Africa, which shows a high negative sensitivity, similar to the results obtained in this study using the MFDI index.

These conditions are directly associated with the variability of the rainy season in the African continent, primarily in the equatorial belt (Le Barbé et al. 2002; Liebmann et al. 2014; Andela and van der Werf 2014; Uele et al. 2017; Ayanlade et al. 2018), as also identified in the study through precipitation simulations based on the ENOS categories. It is worth noting that previous studies have linked the seasonal variability of precipitation to the influence of ENOS (Andela and van der Werf 2014; Uele et al. 2017; Ayanlade et al. 2018). Studies based on orbital products, for example, Jiang et al. (2020), identified long-term fire trends based on burned areas from the MODIS product

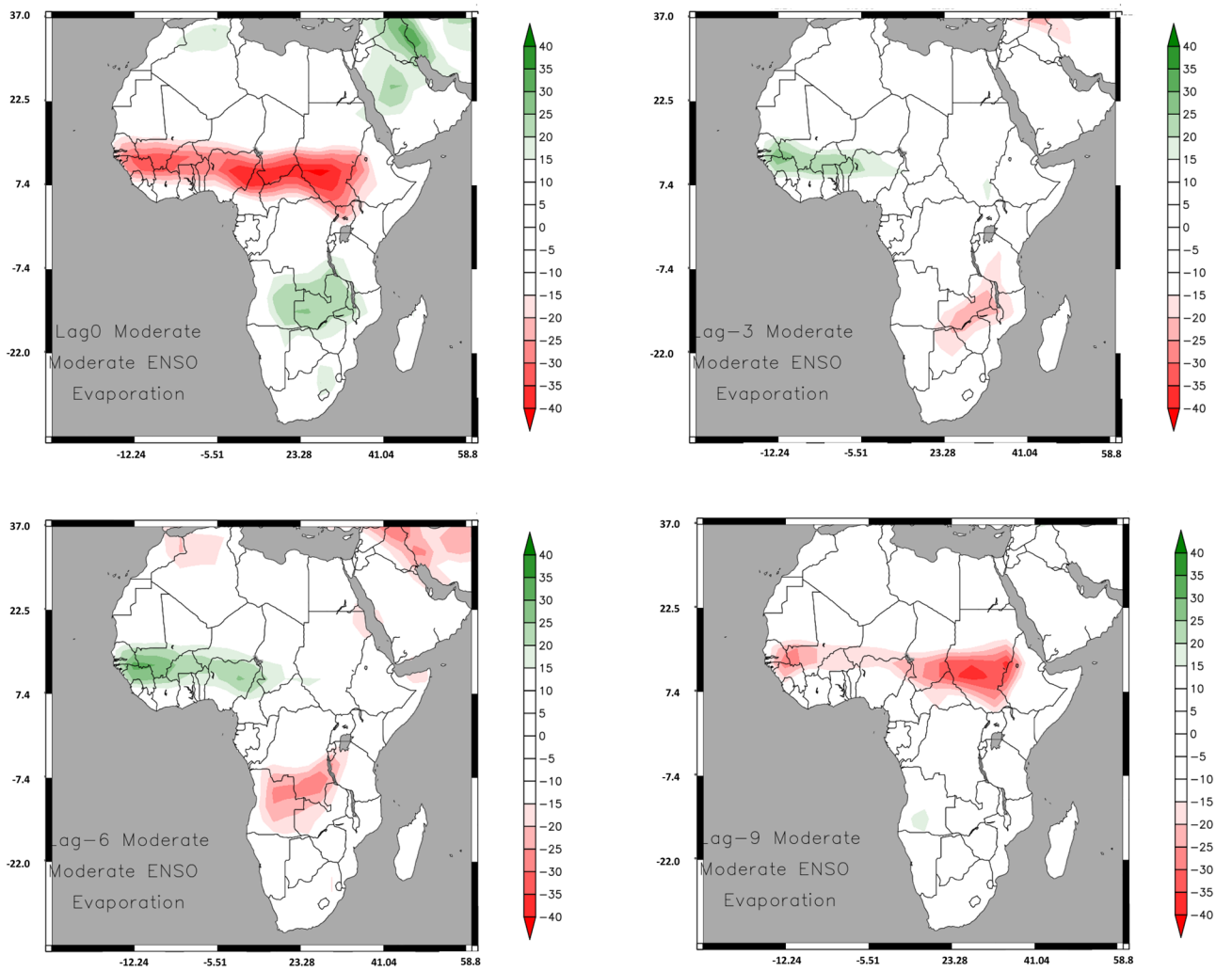

Fig. 7 Evaporation simulations (mm) moderate ENSO category

(MOD13C1) and fire emissions from the Global Fire Emissions Database (GFED4s) in Central Africa. Joshi and Sukumar (2021), using Vegetation Type Fractions (MOD12Q1/MCD12C1) and Gross Primary Productivity (GPP) (MOD17A1) products, indicated an increase in the Central and Southern regions of Africa. The use of MDFI and the SPEEDY-HYCOM model showed similar results to previous studies for both mentioned regions.

This increased risk is directly linked to the soil moisture conditions, characterized by a high deficit in moisture. Consequently, it contributes significantly to the expansion of the MFDI risk area (Rojas et al. 2011; Dong-Yun et al. 2013; Cao et al. 2015; Burton et al. 2020). Our simulations on the precipitation and evaporation, since ecosystems largely depend on their distribution space–time in Africa (Konapala et al. 2020), with time lags (0, 3, 6, and 9; i.e., with a 0 to 9-month lag) for the above-mentioned El Niño categories.

According to De Sales (2019), the rainfall deficit is linked to evapotranspiration, resulting from a decrease in the net surface radiation balance, followed by a reduction in precipitation, especially in metropolitan areas with high population density in Southern Africa. Burton et al. (2020) also suggested a potential intensification in the frequency and extent of forest fires due to the projected population increase along with global warming in Africa. These factors are expected to amplify the impacts of forest fires based on the seasonal variability of rainfall and evaporation in the region, aligning with the findings in this study. The scientific and practical importance of understanding fires and their implications for the current and future climate of Southern Africa is underscored, with results similar to those in the study, except for the population factor.

Uele et al. (2017) reported negative anomalies of precipitation, as well as Sedano et al. (2020) used multitemporal Sentinel-2 imagery to monitor and quantify forest

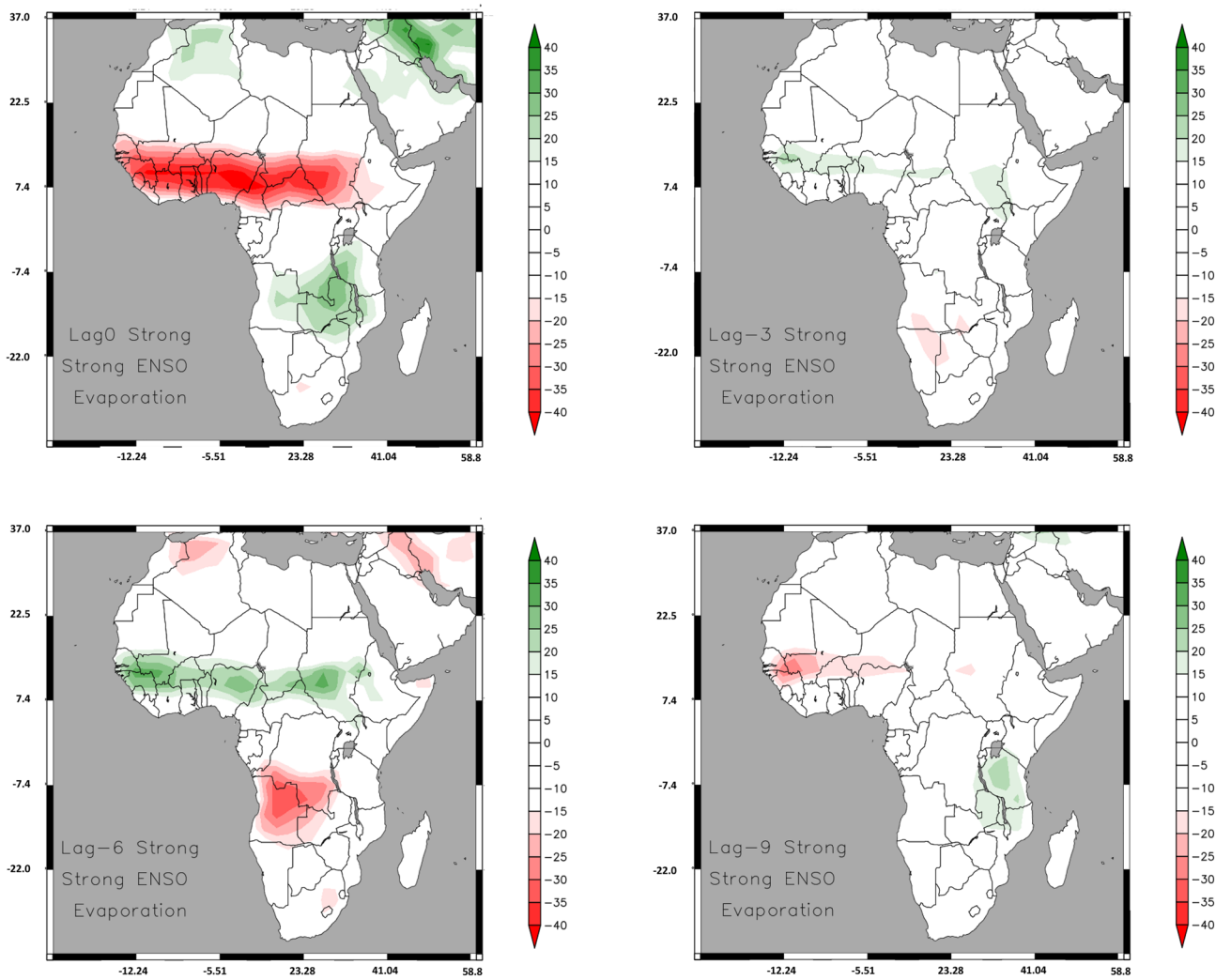

Fig. 8 Evaporation simulations (mm) strong ENSO category

degradation extent, both in Southern Africa. Previously, Andela and van der Werf (2014) found that the changes in precipitation were driven by ENSO and contributed to the increase in wildfires over southern Africa. Burton et al. (2020) used the coupled fire-vegetation model (JULES-INFERNO) to assess the impact of El Niño 2015/16 on fire dynamics in Africa and the results indicated that there was an increase in area burned under El Niño conditions, mainly concerning the precipitation in southern Africa, being drier compared to the rest of the mainland, corroborating the result obtained for lag-6, regardless of El Niño category. Chen et al. (2017) found that the reductions in precipitation and terrestrial water storage have increased emissions from pantropical forest fires during and after El Niño compared to La Niña, being confirmed in the study using the simulations of precipitation and evaporation variables, mainly in Africa Central and Southern.

The SPEEDY-HYCOM model enabled the observation of the effects on Southern and Central Africa concerning the expansion of fire risk categories through MDFI. These changes can pose a threat to various biomes and directly impact the populations of the countries in both regions mentioned above. The results are supported by the findings of Rohat et al. (2019) who evaluated socioeconomic and climatic scenarios in the Central Africa region, which will be drastically affected by climate change, especially in terms of exposure to extreme temperatures resulting from anthropogenic actions and urbanization processes. Heat waves and prolonged droughts occurring in the African continent intensify the risk of fire as indicated in recent studies by Richardson et al. (2022) and Senande-Rivera et al. (2022).

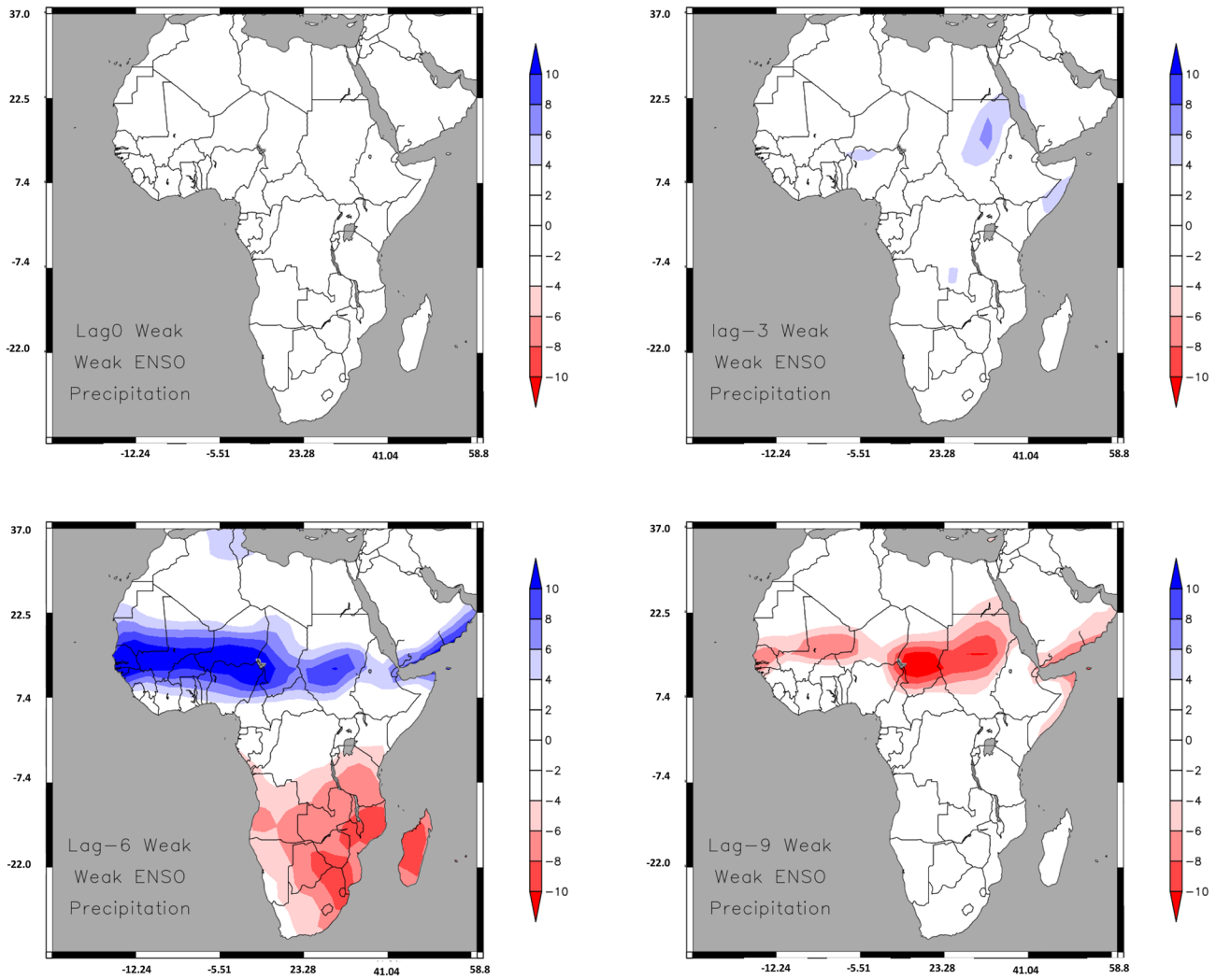

Fig. 9 Precipitation simulations (mm) weak ENSO category

5 Conclusions

The MFDI simulated by the coupled model SPEEDY-HYCOM for three categories of El Niño (Weak, Moderate, and Strong) in lagged months indicated that there are marked differences between the categories regarding the danger of fire in Africa. The El Niño Weak presents variability between maximum risk as well as time lags mainly in Southern African countries, where sustainable fire management should be encouraged, followed by emissions reduction and real-time monitoring of fires during El Niño events.

El Niño Moderate is similar to El Niño Weak, the exceptions are lag-6 and the highest occurrence in the equatorial zone of Africa, which in turn deserves attention by authorities and managers regarding environmental factors in relation to the occurrence of fire during the performance of both the El Niño categories. El Niño Strong occurs in East Africa, with maximum fire risk, regardless of time lags, such a condition is necessary for mitigation actions, as the category implies maximum danger of fire in Africa. Precipitation and evaporation simulations via the SPEEDY-HYCOM model point out that the El Niño categories act with intensity and duration different in Africa. However, Central Africa and especially Africa Austral deserves all the attention in relation to El Niño, with emphasis on the lags 0 and 6 (evaporation) and 0, 6, and 9 (precipitation). In summary, the SPEEDY-HYCOM is perfectly applicable using the classic and operational fire hazard index, as well as in the evaluation of the variability of the climatic conditions and their spatial distribution in Africa during the warm phase of ENSO.

This study utilizes the SPEEDY-HYCOM climatic model to assess the Meteorological Fire Danger Index (MFDI) and highlights distinct advantages compared to other methods for detecting wildfire risk in vegetated areas. The accuracy and predictive capabilities are

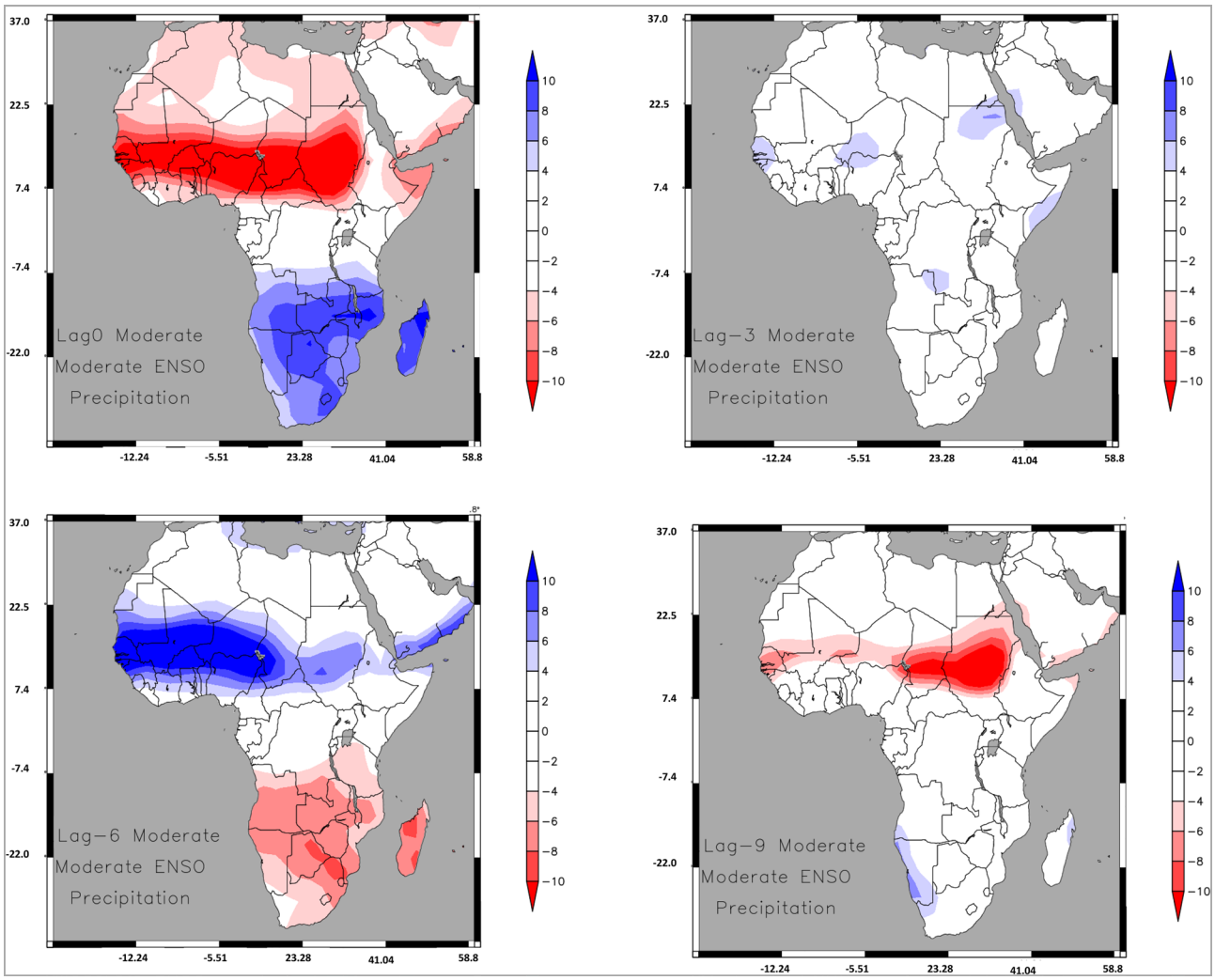

Fig. 10 Precipitation simulations (mm) moderate ENSO category

significantly enhanced with the use of this model, providing a more effective approach to wildfire management and prevention in vegetated environments. These findings have significant implications for the safety and conservation of affected areas.

Initially, the study emphasized the need to identify the factor that exerts the greatest influence on the circumstances that promote the occurrence of forest fires in environments affected by El Niño. Understanding this critical component is fundamental for formulating effective strategies for prevention and mitigation. Furthermore, a more in-depth examination of these findings is essential to assess the socio-environmental consequences caused by forest fires resulting from El Niño events. These consequences have the potential to impact not only biodiversity and ecosystem health but also local communities, the economy, and air quality. It is also necessary to investigate La Niña events in the African continent using not only coupled ocean–atmosphere models but also satellite-derived data on burned areas, land use, and census data, with a particular focus on population density.

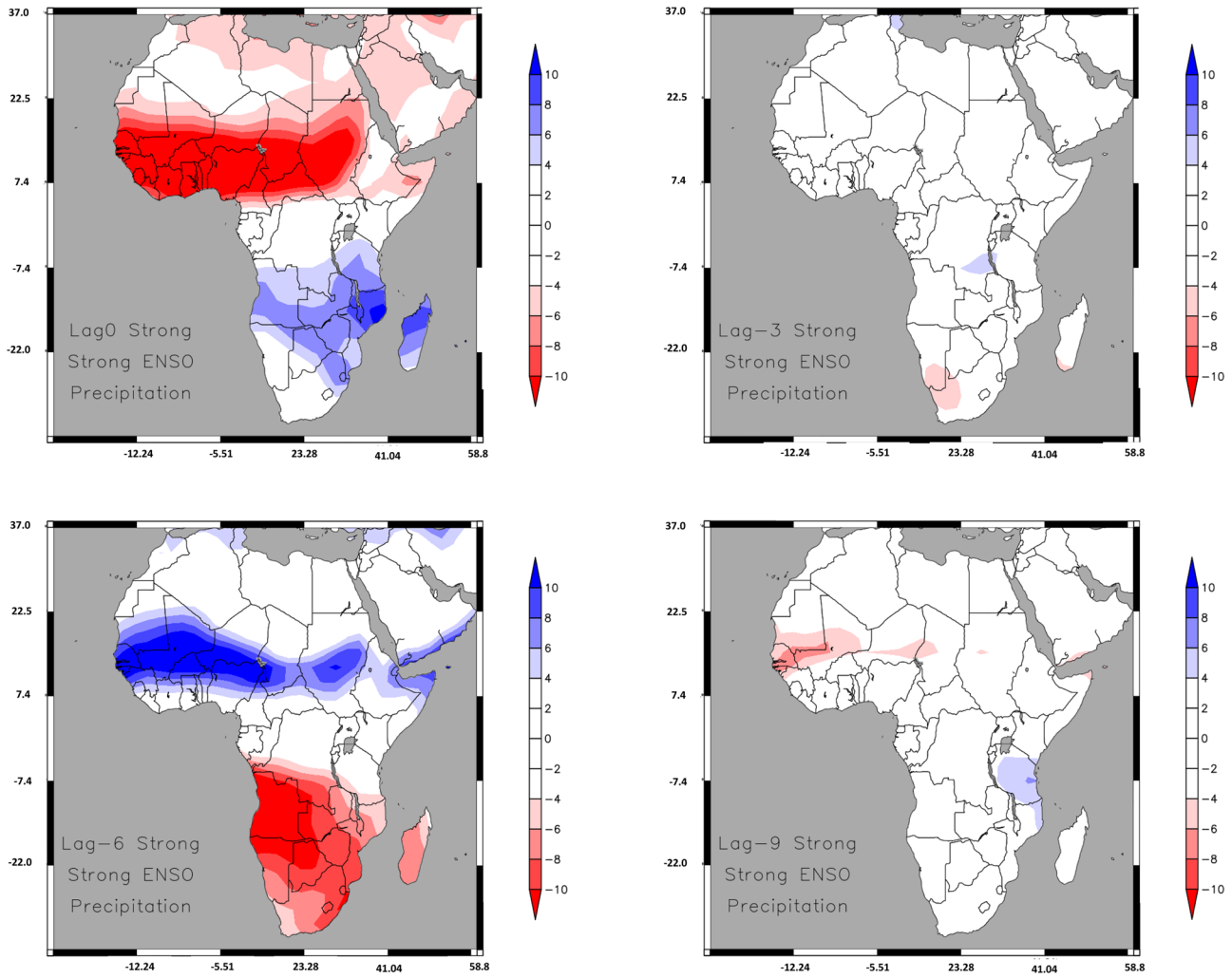

Fig. 11 Precipitation simulations (mm) strong ENSO category

Acknowledgements Authors acknowledge to the Editor of the Journal. SS and BL were supported by the NKFI K138079 and the RRF 2.3.1 21 2022 00008 projects. Authors are also thankful to the developer of SPEEDY and HYCOM models.

Author Contributions José Francisco de Oliveira-Júnior: conceptualization; analysis, writing; David Mendes: supervision, analysis, writing; Szabo Szilard: drafting, proof read; Sudhir Kumar Singh: drafting, editing, proof read; Punyawi Jamjareegulgarn: data preparation, drafting; Kelvy Rosalvo Alencar Cardoso: conceptualization, drafting; Laszlo Bertalan: drafting, editing, proof read; Marcos Vinícius da Silva: analysis, figure preparation; Alexandre Maniçoba da Rosa Ferraz Jardim: data curation, drafting; Jhon Lennon Bezerra da Silva: analysis, drafting; Gustavo Bastos Lyra: writing, figure preparation; Marcel Carvalho Abreu: discussion; figure preparation; Washington Luiz Félix Correia Filho: table creation, editing; Amaury de Sousa: drafting, editing; Dimas de Barros Santiago: data curation, editing; Iwldson Guilherme da Silva Santos: drafting, reviewing; Vafaeva Khristina Maksudovna: data preparation; reviewing; editing. All authors read the manuscript and agreed on its content.

Funding Open access funding provided by University of Debrecen. SS and BL were supported by the NKFI K138079 and the RRF 2.3.1 21 2022 00008 projects.

Availability of Data and Materials Data will be made available on reasonable request.

Declarations

Conflict of interest The authors declare no competing interests.

Ethics approval and consent to participate Not applicable.

Consent for publication Not applicable.

References

Abreu MC, Souza Fraga M, Lyra GB, Oliveira Júnior JF, Jesús Villar-Hernández B, Souza A, Zeri M (2023) Long-term trend analysis in annual, seasonal and monthly rainfall in East Northeast of Brazil and the influence of modes of climate variability. Int J Climatol. https://doi.org/10.1002/joc.8274

Adamson G (2022) El Niño without 'El Niño'? Path dependency and the definition problem in El Niño southern oscillation research. Environ Plan E Nat Space. https://doi.org/10.1177/25148486221120546

Andela N, van der Werf GR (2014) Recent trends in African fires driven by cropland expansion and El Niño to La Niña transition. Nat Clim Change 4:791–795. https://doi.org/10.1038/nclimate2313

Ansari A, Rao KS, Jain AK (2023a) Application of MICROZONATION TOWARDS SYSTEM-WIDE SEISMIC RISK ASSESSMENT OF RAILWAY NEtwork. Transp Infrast Geotech 10:1–24. https://doi.org/10.1007/s40515-023-00317-y

Ansari A, Rao KS, Jain AK (2023b) Seismic response and fragility evaluation of circular tunnels in the Himalayan region: Implications for post-seismic performance of transportation infrastructure projects in Jammu and Kashmir. Tunnel. Undergr Sp Technol 137:1–13. https://doi.org/10.1016/j.tust.2023.105118

Archibald S, Roy DP, Van Wilgen BW, Scholes RJ (2009) What limits fire? An examination of drivers of burnt area in Southern Africa. Glob Change Biol 15:613–630. https://doi.org/10.1111/j.1365-2486.2008.01754.x

Archibald S, Nickless A, Govender N, Scholes RJ, Lehsten V (2010) Climate and the inter-annual variability of fire in southern Africa: a meta-analysis using long-term field data and satellite-derived burnt area data. Glob Ecol Biogeogr 19:794–809. https://doi.org/10.1111/j.1466-8238.2010.00568.x

Archibald S, Staver CA, Levin SA (2011) Evolution of human-driven fire regimes in Africa. PNAS 109(3):847–852. https://doi.org/10.1073/pnas.1118648109

Ayanlade A, Radeny M, Morton JF, Muchaba T (2018) Rainfall variability and drought characteristics in two agro-climatic zones: an assessment of climate change challenges in Africa. Sci Total Environ 630:728–737. https://doi.org/10.1016/j.scitotenv.2018.02.196

Beck HE, Zimmermann NE, McVicar TR, Vergopolan N, Berg A, Wood EF (2018) Present and future Köppen-Geiger climate classification maps at 1-km resolution. Sci Data 5:1–12. https://doi.org/10.1038/sdata.2018.214

Berlato MA, Farenzena H, Fontana DC (2005) Associação entre El Niño Oscilação Sul e a produtividade do milho no Estado do Rio Grande do Sul. Pesqui Agropecu Bras 40:423–432. https://doi.org/10.1590/S0100-204X2005000500001

Bleck R (2002) An oceanic general circulation model framed in hybrid isopycnic - Cartesian coordinates. Ocean Model 4:55–88. https://doi.org/10.1016/S1463-5003(01)00012-9

Bowman DM, Balch JK, Artaxo P, Bond WJ, Carlson JM, Cochrane MA, Pyne SJ (2009) Fire in the earth system. Science 324:481–484. https://doi.org/10.1126/science.1163886

Burton C, Betts RA, Jones CD, Feldpausch TR, Cardoso M, Anderson LO (2020) El Niño driven changes in global fire 2015/16. Front Earth Sci 8:199. https://doi.org/10.3389/feart.2020.00199

Camia A, Bovio G, Aguado I, Stach N (1999) Meteorological fire danger indices and remote sensing. In: Remote Sensing of Large Wildfires: in the European Mediterranean Basin, 39–59. https://doi.org/10.1007/978-3-642-60164-4_4

Cao X, Meng Y, Chen J (2015) Mapping grassland wildfire risk of the world. World atlas of natural disaster risk, 277–283. https://doi.org/10.1007/978-3-662-45430-5_15

Carter TS, Heald CL, Cappa CD, Kroll JH, Campos TL, Coe H, Wu H (2021) Investigating carbonaceous aerosol and its absorption properties from fires in the Western United States (WE-CAN) and Southern Africa (ORACLES and CLARIFY). J Geophys Res Atmos 126:e2021JD034984. https://doi.org/10.1029/2021JD034984

Chen Y, Morton DC, Andela N, Van Der Werf GR, Giglio L, Randerson JT (2017) A pan-tropical cascade of fire driven by El Niño/Southern Oscillation. Nat Clim Change 7:906–911. https://doi.org/10.1038/s41558-017-0014-8

De Sales F, Okin GS, Xue Y, Dintwe K (2019) On the effects of wildfires on precipitation in Southern Africa. Clim Dyn 52:951–967. https://doi.org/10.1007/s00382-018-4174-7

Dong-Yun K, Valerie T, Jenny O, Matthew W, Nicolle C (2013) Statistical trend and change-point analysis of land-cover-change patterns in East Africa. Int J Remote Sens 34:6636–6650. https://doi.org/10.1080/01431161.2013.804224

Giglio L, Van der Randerson JT, Werf GR (2013) Analysis of daily, monthly, and annual burned area using the fourth-generation global fire emissions database (GFED4). J Geophys Res 118:317–328. https://doi.org/10.1002/jgrg.20042

Gobo JPA, Wollmann CA, Celuppi MC, Galvani E, Faria MR, Mendes D, Oliveira-Júnior JF, Gonçalves FLT (2022) The bioclimate present and future in the state Of São Paulo/Brazil: space-time analysis of human thermal comfort. Sustain Cities Soc 78:103611. https://doi.org/10.1016/j.scs.2021.103611

Griffiths IL (2013) The atlas of African affairs. Routledge

Held I, Suarez M (1978) A two-level primitive equation atmosphere model designed for climate sensitivity experiments. J Atmos Sci 35:206–229. https://doi.org/10.1175/1520-0469(1978)035%3c0206:ATLPEA%3e2.0.CO;2

Huang B, Menne MJ, Boyer T, Freeman E, Gleason BE, Lawrimore JH, Liu C, Rennie JJ, Schreck C, Sun F, Vose R, Williams CN, Yin X, Zhang H-M (2020) Uncertainty estimates for sea surface temperature and land surface air temperature in NOAA Global Temp version 5. J Clim 33:1351–1379. https://doi.org/10.1175/JCLI-D-19-0395.1

Jiang Y, Zhou L, Raghavendra A (2020) Observed changes in fire patterns and possible drivers over Central Africa. Environ Res Lett 15:0940b8. https://doi.org/10.1088/1748-9326/ab9db2

Jimenez JC, Libonati R, Peres LF (2018) Droughts over Amazonia in 2005, 2010, and 2015: a cloud cover perspective. Front Earth Sci 6:227. https://doi.org/10.3389/feart.2018.00227

Joshi J, Sukumar R (2021) Improving prediction and assessment of global fires using multilayer neural networks. Sci Rep 11:3295. https://doi.org/10.1038/s41598-021-81233-4

Kalnay E, Kanamitsu M, Kistler R, Collins W, Deaven D, Gandin L, Iredell M, Saha S, White G, Woollen J, Zhu Y, Chelliah M, Ebisuzaki W, Higgins W, Janowiak J, Mo KC, Ropelewski C, Wang J, Leetmaa A, Reynolds R, Jenne R, Joseph D (1996) The

NCEP/NCAR 40-Year Reanalysis Project. Bull Am Meteorol Soc 77:437–472. https://doi.org/10.1175/1520-0477(1996)077%3c0437:TNYRP%3e2.0.CO;2

Konapala G, Mishra AK, Wada Y, Mann ME (2020) Climate change will affect global water availability through compounding changes in seasonal precipitation and evaporation. Nat Commun 11:3044. https://doi.org/10.1038/s41467-020-16757-w

Kotsuki S, Miyoshi T, Kondo K, Potthast R (2022) A local particle filter and its Gaussian mixture extension implemented with minor modifications to the LETKF. Geosci Model Dev 15:8325–8348. https://doi.org/10.5194/gmd-15-8325-2022

Kucharski F, Molteni F, Bracco A (2005) Decadal interactions between the western tropical Pacific and the North Atlantic Oscillation. Clim Dyn 26:79–91. https://doi.org/10.1007/s00382-005-0085-5

Le Barbé L, Lebel T, Tapsoba D (2002) Rainfall variability in West Africa during the Years 1950–90. J Clim 15:187–202. https://doi.org/10.1175/1520-0442(2002)015%3c0187:RVIWAD%3e2.0.CO;2

Liebmann B, Hoerling MP, Funk C, Bladé I, Dole RM, Allured D, Quan X, Pegion P, Eischeid JK (2014) Understanding recent eastern horn of Africa rainfall variability and change. J Clim 27:8630–8645. https://doi.org/10.1175/JCLI-D-13-00714.1

Loudermilk EL, O'Brien JJ, Goodrick SL, Linn RR, Skowronski NS, Hiers JK (2022) Vegetation's influence on fire behavior goes beyond just being fuel. Fire Ecol 18:9. https://doi.org/10.1186/s42408-022-00132-9

Molteni F (2003) Atmospheric simulations using a GCM with simplified physical parametrizations. I: model climatology and variability in multi-decadal experiments. Clim Dyn 20:175–191. https://doi.org/10.1007/s00382-002-0268-2

Oliveira-Júnior JF, Mendes D, Correia Filho WLF, Silva Junior CA, Gois G, Jardim AMRF, Silva MV, Lyra GB, Teodoro PE, Pimentel LCG, Lima M, Santiago DB, Rogério JP, Marinho AAR (2021) Fire foci in South America: impact and causes, fire hazard and future scenarios. J South Am Earth Sci 112:103623. https://doi.org/10.1016/j.jsames.2021.103623

Peel MC, Finlayson BL, McMahon TA (2007) Updated world map of the Köppen-Geiger climate classification. Hydrol Earth Syst Sci 11:1633–1644. https://doi.org/10.5194/hess-11-1633-2007

Philander SG (1998) Who is El Niño? Eos Trans Am Geophys Union 79:170–170

Richardson D, Black AS, Irving D, Matear RJ, Monselesan DP, Risbey JS, Tozer CR (2022) Global increase in wildfire potential from compound fire weather and drought. Npj Clim Atmos Sci 5:23. https://doi.org/10.1038/s41612-022-00248-4

Rohat G, Flacke J, Dosio A, Dao H, van Maarseveen M (2019) Projections of human exposure to dangerous heat in African cities under multiple socioeconomic and climate scenarios. Earth's Future 7:528–546. https://doi.org/10.1029/2018EF001020

Rojas O, Rembold F, Delincé J, Léo O (2011) Using the NDVI as auxiliary data for rapid quality assessment of rainfall estimates in Africa. Int J Remote Sens 32:3249–3265. https://doi.org/10.1080/01431161003698260

Russell-Smith J, Yates C, Vernooij R, Eames T, van der Werf G, Ribeiro N, Johnston S (2021) Opportunities and challenges for savanna burning emissions abatement in southern Africa. J Environ Manage 288:112414. https://doi.org/10.1016/j.jenvman.2021.112414

Saha MV, D'Odorico P, Scanlon TM (2019) Kalahari wildfires drive continental post-fire brightening in sub-Saharan Africa. Remote Sens 11:1090. https://doi.org/10.3390/rs11091090

Sedano F, Lisboa S, Duncanson L, Ribeiro N, Sitoe A, Sahajpal R, Tucker C (2020) Monitoring intra and inter annual dynamics of forest degradation from charcoal production in Southern Africa with Sentinel–2 imagery. Int J Appl Earth Obs Geoinf 92:102184. https://doi.org/10.1016/j.jag.2020.102184

Senande-Rivera M, Insua-Costa D, Miguez-Macho G (2022) Spatial and temporal expansion of global wildland fire activity in response to climate change. Nat Commun 13:1208. https://doi.org/10.1038/s41467-022-28835-2

Spinoni J, Barbosa P, Cherlet M, Forzieri G, McCormick N, Naumann G, Dosio A (2021) How will the progressive global increase of arid areas affect population and land-use in the 21st century? Glob Planet Change 205:103597. https://doi.org/10.1016/j.gloplacha.2021.103597

Strydom S, Savage MJ (2016) A spatio-temporal analysis of fires in South Africa. S Afr J Sci 112:1–8. https://doi.org/10.17159/sajs.2016/20150489

Thomson A (2022) An introduction to African politics. Taylor & Francis

Trenberth KE (1997) The definition of El Nino. Bull Am Meteorol Soc 78:2771–2778. https://doi.org/10.1175/1520-0477(1997)078%3c2771:TDOENO%3e2.0.CO;2

Trollope WSW, Trollope LA (1997) Fire effects and management in African grasslands and savannas. Range and Animal Science and Resource Management (Vol II). Encyclopedia of Life Support Systems, Nelspruit

Uele DI, Lyra GB, Oliveira Júnior JF (2017) Variabilidade Espacial e Intranual das Chuvas na Região Sul de Moçambique, África Austral. Rev Bras Meteorol 32:473–484. https://doi.org/10.1590/0102-77863230013

Varotsos CA, Tzanis CG, Sarlis NV (2016) On the progress of the 2015–2016 El Niño event. Atmos Chem Phys 16:2007–2011. https://doi.org/10.5194/acp-16-2007-2016

Vitolo C, Di Giuseppe F, Barnard C, Coughlan R, San-Miguel-Ayanz J, Libertá G, Krzeminski B (2020) ERA5-based global meteorological wildfire danger maps. Sci Data 7:216. https://doi.org/10.1038/s41597-020-0554-z

Wan C, Roy SS (2022) Geospatial characteristics of fire occurrences in southern hemispheric Africa and Madagascar during 2001–2020. J for Res 1:1–11. https://doi.org/10.1007/s11676-022-01487-0

Wei F, Wang S, Fu B, Brandt M, Pan N, Wang C, Fensholt R (2020) Nonlinear dynamics of fires in Africa over recent decades controlled by precipitation. Glob Change Biol 26:4495–4505. https://doi.org/10.1111/gcb.15190

Wei F, Wang S, Brandt M, Fu B, Meadows ME, Wang L, Fensholt R (2021) Responses and feedbacks of African dryland ecosystems to environmental changes. Curr Opin Environ Sust 48:29–35. https://doi.org/10.1016/j.cosust.2020.09.004

Xie X, He B, Guo L, Huang L, Hao X, Zhang Y, Wang S (2022) Revisiting dry season vegetation dynamics in the Amazon rainforest using different satellite vegetation datasets. Agric for Meteorol 312:108704. https://doi.org/10.1016/j.agrformet.2021.108704

Xu H, Abdul-Kadar F, Gao P (2016) An information model for managing multi-dimensional gridded data in a GIS. IOP Conf Ser Earth Environ Sci 34:012041. https://doi.org/10.1088/1755-1315/34/1/012041

Authors and Affiliations

José Francisco de Oliveira-Júnior[1] · David Mendes[2] · Szilard Szabo[3] · Sudhir Kumar Singh[4] · Punyawi Jamjareegulgarn[5] · Kelvy Rosalvo Alencar Cardoso[1] · Laszlo Bertalan[3] · Marcos Vinicius da Silva[6] · Alexandre Maniçoba da Rosa Ferraz Jardim[7] · Jhon Lennon Bezerra da Silva[7] · Gustavo Bastos Lyra[6] · Marcel Carvalho Abreu[6] · Washington Luiz Félix Correia Filho[8] · Amaury de Sousa[9] · Dimas de Barros Santiago[10] · Iwldson Guilherme da Silva Santos[10] · Vafaeva Khristina Maksudovna[11]

✉ Szilard Szabo
szabo.szilard@science.unideb.hu

José Francisco de Oliveira-Júnior
jose.junior@icat.ufal.br

David Mendes
david.mendes@ufrn.br

Sudhir Kumar Singh
sudhirinjnu@gmail.com

Punyawi Jamjareegulgarn
punyawi.ja@kmitl.ac.th

Kelvy Rosalvo Alencar Cardoso
kelvy.cardoso@icat.ufal.br

Laszlo Bertalan
bertalan@science.unideb.hu

Marcos Vinicius da Silva
marcos.viniciussilva@ufrpe.br

Alexandre Maniçoba da Rosa Ferraz Jardim
alexandremrfj@gmail.com

Jhon Lennon Bezerra da Silva
jhonlennoigt@hotmail.com

Gustavo Bastos Lyra
gblyra@gmail.com

Marcel Carvalho Abreu
marcelc.abreu@gmail.com

Washington Luiz Félix Correia Filho
washington.correia@furg.br

Amaury de Sousa
amaury.souza@ufms.br

Dimas de Barros Santiago
dimas.barros91@gmail.com

Iwldson Guilherme da Silva Santos
iwldson@gmail.com

Vafaeva Khristina Maksudovna
vafaeva.hm@edu.spbstu.ru

[1] Institute of Atmospheric Sciences (ICAT), Federal University of Alagoas (UFAL), Maceió, Alagoas 57072-260, Brazil

[2] Post-Graduate Program in Aerospace Engineering, PPGEA, Federal University of Rio Grande do Norte, UFRN, Lagoa Nova University Campus, Natal, RN, Brazil

[3] Department of Physical Geography and Geoinformatics, Faculty of Sciences and Technology, Institute of Geosciences, University of Debrecen, Debrecen, Egyetem tér 1 4032, Hungary

[4] K. Banerjee Centre of Atmospheric and Ocean Studies, University of Allahabad, 211002, Prayagraj, UP, India

[5] King Mongkut's Institute of Technology Ladkrabang, Prince of Chumphon Campus, Chumphon 86160, Thailand

[6] Department of Environmental Sciences (DCA), Forestry Institute (IF), Federal Rural University of Rio de Janeiro (UFRRJ), Seropédica, Rio de Janeiro 23890-000, Brazil

[7] Department of Agricultural Engineering, Federal Rural University of Pernambuco, Recife , Pernambuco, Brazil

[8] Institute of Mathematics, Statistics and Physics (IMEF), Federal University of Rio Grande (FURG), Av. Itália km 8, Carreiros, Rio Grande, Rio Grande do Sul 96203-900, Brazil

[9] Universidade Federal de Mato Grosso do Sul, Campo Grande, MS, Brazil

[10] Postgraduate Program in Meteorology, Academic Unit of Atmospheric Sciences (UACA), Federal University of Campina Grande (UFCG), Campina Grande, Paraíba 58429-140, Brazil

[11] Peter the Great St. Petersburg Polytechnic University, 195251 St. Petersburg, Russia